JOURNAL OF Materials CHEMISTRY

Binary nitrides α-M_3N_2 (M = Be, Mg, Ca): a theoretical study

E. Orhan,[a] S. Jobic,[b] R. Brec,[b] R. Marchand*[a] and J.-Y. Saillard*[c]

[a]*Laboratoire Verres et Céramiques, UMR CNRS 6512, Institut de Chimie de Rennes, Université de Rennes 1, Campus de Beaulieu, 35042 Rennes cedex, France*
[b]*Laboratoire de Chimie des Solides, Institut Jean Rouxel, 2 rue de la Houssinière, BP 32229, 44322 Nantes cedex 3, France*
[c]*Laboratoire de Chimie du Solide et Inorganique Moléculaire, UMR CNRS 6511, Institut de Chimie de Rennes, Université de Rennes 1, Campus de Beaulieu, 35042 Rennes cedex, France*

Received 10th April 2002, Accepted 22nd May 2002
First published as an Advance Article on the web 28th June 2002

Detailed results of DFT band structure calculations for the α-M_3N_2 (M = Be, Mg, Ca) binary nitrides are reported. The cell parameters and atomic positions were optimized with the molecular dynamics pseudopotential approach of the Vienna *ab initio* simulation program (VASP). The optimized structures were subsequently calculated with the WIEN97 program, based on the full potential linearised augmented plane waves (FP-LAPW) method, within the framework of density functional theory (DFT). As expected, the valence band is composed of the nitrogen 2p states, while the conduction band comprises the metallic states. The band gap was found to decrease when going from Be to Mg and Ca. This counterintuitive result is due to the existence of a significant anion–cation covalent interaction which decreases when going from Be to Mg and Ca. The electronic structures of the mixed nitride $CaMg_2N_2$ and of the hypothetical α-M_3N_2 (M = Sr, Ba) phases are also discussed in the light of the above results.

Introduction

In recent years, nitride and oxynitride materials have become a rapidly growing field of interest, for example, with respect to their potential use as industrial non-toxic pigments. As a matter of fact, Ta_3N_5 will be industrially produced as a colored pigment in the near future.[1,2] The mechanism involved in these semi-conducting pigments is a band-to-band transition between the fully occupied valence band and the empty conduction band.[3] The width of the corresponding band gap is important, since it determines the energy threshold from which radiation will be absorbed. The nature of the band gap transition (direct or indirect) also plays a role in the color characteristics, in relation to the allowed or forbidden nature of the HOMO–LUMO transition. In this work, we will consider some alkaline earth metal nitrides (M_3N_2, with M = Be, Mg and Ca) to study the nature of the band gaps, as well as the bonding properties of M, in relation to the ionic/covalent character of the M–N bonds, focusing on the cubic (α) variety. It should be noted that Hartree–Fock (HF) calculations on α-Be_3N_2 and α-Mg_3N_2 with *a posteriori* density functional theory (DFT) corrections have been published recently by Moreno Armenta *et al.*,[4] and that Fang *et al.* have published *ab initio* band structure calculations (using the local spherical waves method) on α-Mg_3N_2.[5]

For the sake of comparison, we also have performed geometry optimization on the hypothetical compounds α-Sr_3N_2 and α-Ba_3N_2, which have not been clearly isolated so far.[6] These two phases have been the subject of many controversial studies,[7–10] but their existence has not been proven yet. Calculations were also carried out on the trigonal mixed nitride $CaMg_2N_2$.[11]

What really triggered our study on the title α-M_3N_2 series is the report that, while α-Be_3N_2 is white in color, α-Mg_3N_2 is yellow and α-Ca_3N_2 red–brown. From usual concepts, and because these three compounds are described in the literature as "ionic nitrides",[6] one expects the more electropositive cation to present a more ionic structure, hence a wider band gap. α-Mg_3N_2 and α-Ca_3N_2 were thus expected to be as white as α-Be_3N_2. We were driven by a desire to understand the differences in the observed colors.

Crystal structures

Two polymorphs of Be_3N_2 are known. The high temperature β-form adopts an hexagonal structure, while the white low temperature α-form crystallizes with the cubic *anti*-bixbyite structure (space group $Ia\bar{3}$), shown in Fig. 1. In this structure, each beryllium atom is tetrahedrally coordinated by nitrogen, while each nitrogen is coordinated by six beryllium atoms. There are two crystallographically different nitrogen atoms in this structure. One of them, N(1), has distorted octahedral coordination [Fig. 2(a) and (b)]: the surrounding nitrogens can be represented [Fig. 2(b)] as a pseudo-cube in which two opposite vertices are empty. The second nitrogen, N(2), has more complex hexacoordination [see Fig. 2(c) and (d)]: the nitrogen coordination can be viewed as corresponding to a strongly distorted cube in which two diagonally opposed nitrogens belonging to one face are missing. Therefore, α-Be_3N_2 can be described as having a structure in which the metal atoms are located in tetrahedral sites of an approximately cubic, deficient, distorted, close-packed array

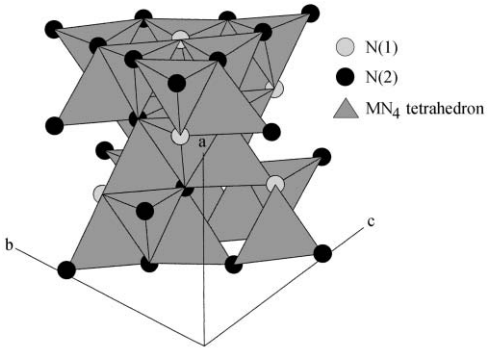

Fig. 1 Crystal structure of M_3N_2.

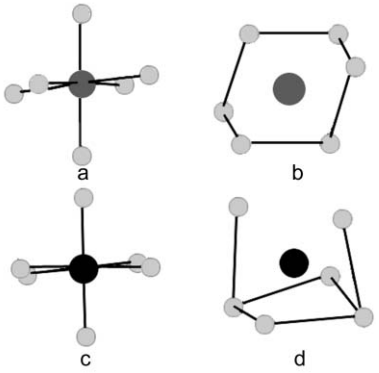

Fig. 2 The two ways of representing the nitrogen environments. Top: N(1); bottom: N(2).

of nitrogen atoms. The cell parameters were determined from X-ray powder diffraction data by Stackelberg and Paulus in 1933;[7] they did not solve the structure but gave approximate values of the crystallographical positions.

The best crystal structure refinement of Mg_3N_2 was recently carried out from neutron time-of-flight powder diffraction data.[12] The phase also has the *anti*-bixbyite structure type. In the two different [MgN_6] polyhedra, one has six N(1)–Mg distances of 2.14 Å, while the other is characterized by three pairs of identical N(2)–Mg distances (2.08, 2.16 and 2.18 Å). The tetrahedron surrounding the Mg atom is distorted, one of the Mg–N bonds being shorter than the other three (2.08 *vs.* 2.14, 2.16 and 2.18 Å).

Ca_3N_2 reportedly exists in three forms: cubic, orthorhombic and pseudo-hexagonal. The cubic α-form (*anti*-bixbyite type) is the only well-characterized variety. The structure of this red–brown compound, refined by X-ray powder diffraction,[13] is close to that of Mg_3N_2, but the sites are less distorted: one [NCa_6] unit has 6 equal N–Ca distances (2.46 Å), and the other has almost equal bonds (4 × 2.45 and 2 × 2.47 Å).

The structure of the mixed nitride $CaMg_2N_2$ has been determined by powder X-ray diffraction.[11] It adopts the trigonal *anti*-La_2O_3 structure (space group $P\bar{3}m1$). The calcium ions lie in almost regular octahedral sites (6 × 2.60 Å) and the magnesium ions in distorted tetrahedral sites (1 × 2.30 ; 3 × 2.13 Å). Each nitrogen atom is surrounded by a pseudo-octahedron made of three Mg and three Ca atoms.

Calculation methods

For the geometry optimizations, we used the *ab initio* total-energy and molecular dynamics program VASP (Vienna *ab initio* simulation program) developed by the Institut für Theoritische Physics of the Technische Universität Wien (who also supplied the pseudopotentials).[14] Vanderbilt-type ultrasoft pseudopotentials were used. The Kohn–Sham orbitals were expanded in plane waves with a kinetic energy cutoff of 36 Ry, while exchange and correlation were treated in the generalized gradient approximation (GGA) using the functional of Perdew *et al.*[15] The Brillouin zone (BZ) was sampled with a 4 × 4 × 4 Monkhorst pack grid, resulting in 24 ***k***-points in the irreducible part centered at gamma (10 × 10 × 6, resulting in 72 ***k***-points for $CaMg_2N_2$). Calculations were performed with relaxation of both atomic positions and lattice parameters.

The computed lattice parameters and atomic positions were then introduced in the full potential linearised augmented plane waves (FP-LAPW) method implemented in the WIEN97 code.[16] In the LAPW method, the unit cell is divided into two types of regions, the atomic spheres centered upon nuclear sites and the interstitial region between the non-overlapping spheres. Inside the atomic spheres, the wave functions are replaced by atomic-like functions, while in the interspheres region, the wave function of a Bloch state is expanded in plane waves. The local density approximation of Perdew *et al.* was used,[15] together with the Perdew–Burke–Ernzerhof GGA potential.[17] The maximum *l* value in the expansion of the basis set inside an atomic sphere was 10 for the computation of the muffin-tin matrix and 4 for the non-muffin-tin matrix element. The convergence of the basis set is controlled by a cutoff parameter, $R_{mt} \times K_{max} = 8$, where R_{mt} is the smallest atomic sphere radius in the unit cell and K_{max} is the magnitude of the largest ***k*** vector. Self-consistency was carried out on a 12 ***k***-point mesh in the irreducible Brillouin zone for the **α**-M_3N_2 series and a 50 ***k***-point mesh for the mixed nitride $CaMg_2N_2$.

Results

The cell parameters of the α-M_3N_2 (M = Be, Mg, Ca) series optimized by the VASP program are not very different from the experimental ones (see Table 1). The corresponding optimized atomic fractional coordinates and bond distances are given in Tables 2 and 3, respectively. They are also in good agreement with the available accurate experimental data. The computed cell parameters of the hypothetical Sr_3N_2 and Ba_3N_2 phases are consistent with the respective sizes of the cations.

Calculations using the WIEN program were carried out on the Be, Mg and Ca phases. Both VASP and WIEN-type calculations provided similar densities of states and band structures. Our results are also qualitatively similar to those obtained previouly on α-Be_3N_2 and α-Mg_3N_2 by Moreno Armenta *et al.* using a combined HF/DFT method.[4] Therefore, only the WIEN densities of states are shown for these three phases in Fig. 3–5 together with their respective projections on M, N(1) and N(2). The WIEN band structures are shown in Fig. 6. As can be seen, the global shape of the density of states is the same for the whole α-M_3N_2 series. As expected, the valence band is predominantly composed of the 2p nitrogen states and the conduction band of the *n*s, *n*p metallic states. The differences between the compounds lie in the width of the valence band and in the size of the forbidden gap between the

Table 2 Calculated atomic fractional coordinates (space group $Ia\bar{3}$) in the α-M_3N_2 (M = Be, Mg, Ca, Sr, Ba) series

Compound	α-Be_3N_2	α-Mg_3N_2	α-Ca_3N_2	Sr_3N_2	Ba_3N_2
M 48e	0.8545	0.8475	0.8892	0.8891	0.8895
	0.1199	0.1180	0.1549	0.1574	0.15921
	0.3862	0.3892	0.1167	0.1155	0.1151
N(1) 8b	0.25	0.25	0.25	0.25	0.25
	0.25	0.25	0.25	0.25	0.25
	0.25	0.25	0.25	0.25	0.25
N(2) 24d	0.5	0.5	0.5	0.5	0.5
	0.75	0.75	0.75	0.75	0.75
	0.4798	0.4690	0.4597	0.4498	0.4439

Table 1 Experimental and calculated values (Å) of the cubic cell parameter for the α-forms (*anti*-bixbyite type) of the M_3N_2 (M = Be, Mg, Ca, Sr, Ba) compounds

Compound	α-Be_3N_2	α-Mg_3N_2	α-Ca_3N_2	Sr_3N_2	Ba_3N_2
a (exp.)	8.134 (1) (ref. 7)	9.9528(1) (ref. 12)	11.467(1) (ref. 13)	—	—
a (calc.)	8.09	9.95	11.42	12.24	13.26

Table 3 Major calculated interatomic distances (Å) for the α-M_3N_2 (M = Be, Mg, Ca, Sr, Ba) series. Available experimental values are given in parentheses (from ref. 12 for α-Mg_3N_2 and ref. 13 for α-Ca_3N_2)

Compound	α-Be_3N_2	α-Mg_3N_2	α-Ca_3N_2	Sr_3N_2	Ba_3N_2
Shortest M···M non-bonding contacts	2.164	2.726 (2.720)	3.144	3.390	3.695
M–N(1) distance	6 × 1.743	6 × 2.143 (2.145)	6 × 2.455 (2.47)	6 × 2.626	6 × 2.841
M–N(2) distances	2 × 1.688	2 × 2.088 (2.084)	2 × 2.449 (2.44)	2 × 2.574	2 × 2.760
	2 × 1.751	2 × 2.159 (2.160)	2 × 2.453 (2.48)	2 × 2.642	2 × 2.860
	2 × 1.785	2 × 2.183 (2.179)	2 × 2.470 (2.49)	2 × 2.691	2 × 2.958

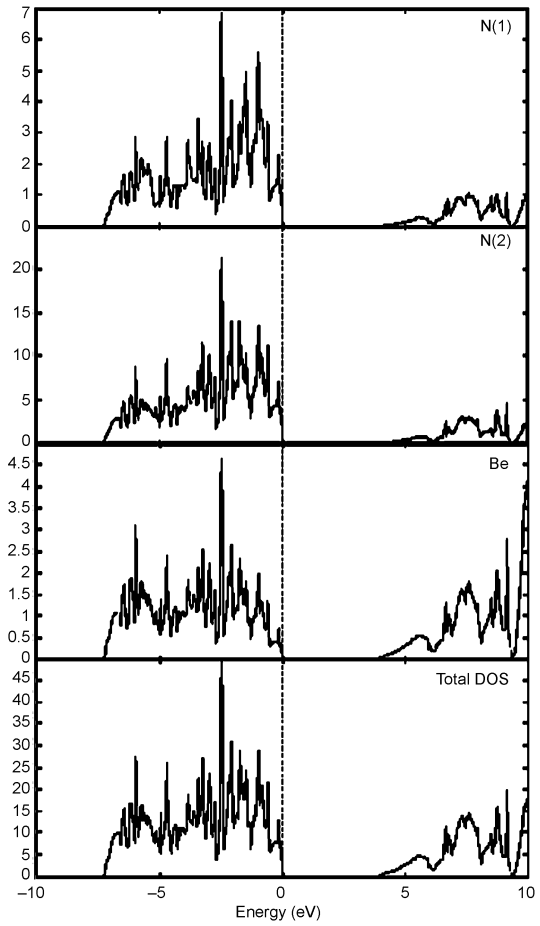

Fig. 3 Projected and total DOS of Be_3N_2.

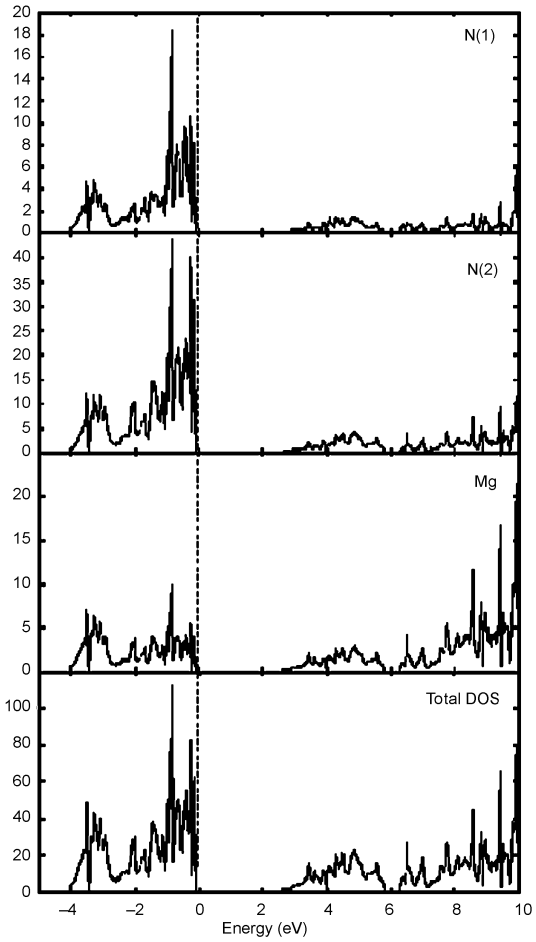

Fig. 4 Projected and total DOS of Mg_3N_2.

valence and conduction band (see Fig. 3–6 and Table 4). All the band gaps are direct gaps at Γ. The widest gap is obtained for Be_3N_2 and it decreases as M descends down the column of the periodic table. A similar trend was found for α-Be_3N_2 and α-Mg_3N_2 by Moreno Armenta *et al.* in their combined HF/DFT study, although their computed band gaps are much larger than ours,[4] as expected, since full DFT calculations are known to underestimate band gaps.[18] The width of the valence band also decreases from Be to Ba (Table 4).

Our major results on the trigonal $CaMg_2N_2$ phase are given in Table 5. The calculated cell parameters (VASP optimization) are very close to the experimental values. The WIEN calculated band gap is 2.05 eV, direct gap at Γ.

Discussion

At first sight, the fact that the computed band gap in the α-M_3N_2 series decreases when M descends the group from Be to Ba is counterintuitive. Indeed, in these compounds, one is tempted to approximate the band gap to the energy difference between the (*n*s,*n*p) states of M^{2+} and the 2p states of N^{3-}, *i.e.* $E_g \approx \Delta E = \varepsilon(ns_M,np_M) - \varepsilon(2p_N)$. This hypothesis is based on the assumption of strongly ionic bonding in the three studied compounds and is illustrated by the simple 2-orbital diagrams given in Fig. 7. In this figure, a 2p occupied orbital of N^{3-} interacts with a vacant *n*s orbital of M^{2+}. Within an almost purely ionic bonding scheme, the interaction between these two orbitals is very small, so that they are barely modified in composition and energy upon interaction. Consequently, the occupied MO is close to 100% N in character and its energy is close to $\varepsilon(2p_N)$, while the vacant MO is close to 100% M in character and its energy is close to $\varepsilon(ns_M)$. In such a simple picture, the former MO represents the valence band and the latter the conduction band. Therefore, the band gap corresponds to the energy difference between these two MOs, *i.e.* is close to the $\varepsilon(ns_M) - \varepsilon(2p_N)$ difference. Since the $\varepsilon(ns_M)$ energy increases when the electronegativity of M decreases, the band gap of α-M_3N_2 is expected to increase when M varies from Be to Ba, a variation which is at odds with the computed band gaps.

To understand the band gap variation in the series, one has to take into account that a significant covalent interaction

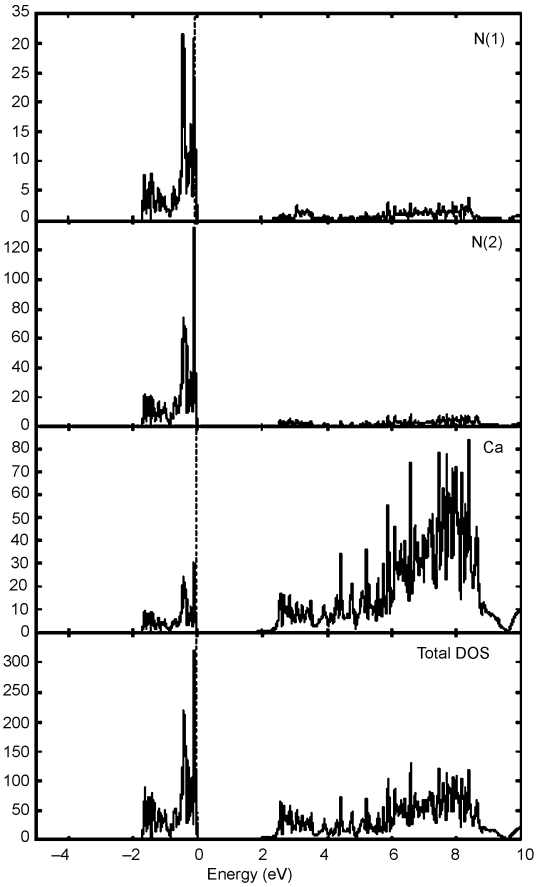

Fig. 5 Projected and total DOS of Ca_3N_2.

between the interacting atomic orbitals is present, as illustrated in Fig. 8. The strength of the interaction between two orbitals depends on their energy difference, ΔE. The smaller this difference, the stronger the interaction. Fig. 8 exemplifies the M = Be and Ca cases, assuming strong covalent interactions, at least in the M = Be case. Since $\Delta E = \varepsilon(ns_M) - \varepsilon(2p_N)$ is smaller when M = Be (see above), the interaction is very strong, both interacting orbitals repel each other strongly, leading to a large band gap. In the case of M = Ca, $\varepsilon(ns_M) - \varepsilon(2p_N)$ is much larger, leading to a much weaker interaction and, therefore, to a smaller band gap.

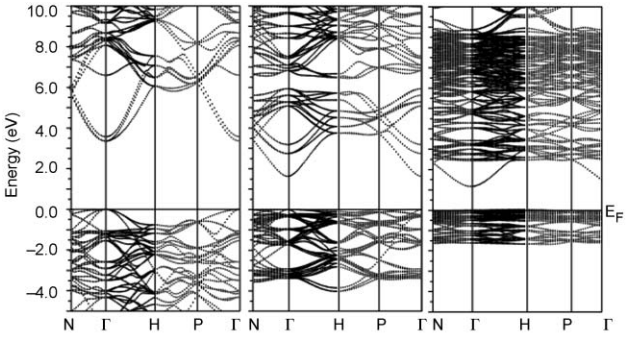

Fig. 6 Band structure of Be_3N_2 (left), Mg_3N_2 (middle) and Ca_3N_2 (right).

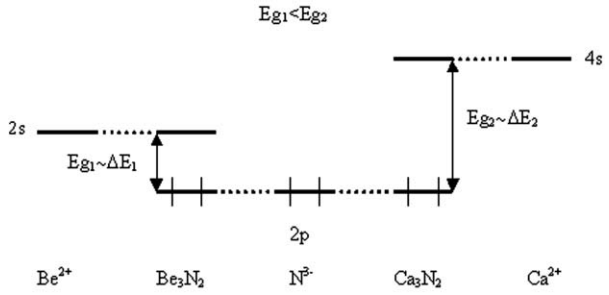

Fig. 7 Simple orbital scheme for Be_3N_2 and Ca_3N_2, assuming negligible covalent interactions.

The strength of the orbital interaction can also be traced in the width of the valence band. The stronger the interaction, the more dispersed the involved bands. It is clear from Table 4 that the valence bandwidth varies in accordance with the orbital interaction strength.

It should be noted that the more covalent character of α-Be_3N_2, as compared to α-Mg_3N_2, has already been outlined by Moreno Armenta *et al.*[4] Our results are also fully consistent with an extended Hückel tight-binding investigation of the series.[19] Being much larger than that of α-Ca_3N_2, the computed band gap of $CaMg_2N_2$ does not fit in the α-M_3N_2 series. This can be easily understood by taking into account the different structure of the mixed nitride phase, as compared to the α-Mg_3N_2 series. In this compound, the hexacoordination of Ca induces a stronger ligand field than for the tetracoordinated M atoms in α-M_3N_2. It turns out that the computed band gap of

Table 4 Calculated valence bandwidth and experimental and calculated band gap in the α-M_3N_2 (M = Be, Mg, Ca, Sr, Ba) series

Compound	α-Be_3N_2	α-Mg_3N_2	α-Ca_3N_2	Sr_3N_2	Ba_3N_2
Color	Colorless	Yellow	Red–brown		
Measured or expected band gap/eV	>3.1 (expected)	2.8 (ref. 5)	1.9 (this work)		
Calculated band gap (WIEN97)/eV	3.35	1.63	1.26		
Calculated band gap (VASP)/eV	5.2	1.85	1.17	0.60	0.47
Calculated valence bandwidth (WIEN97)/eV	7.21	3.89	1.66		
Calculated valence bandwidth (VASP)/eV	7.61	4.12	1.90	1.80	1.53

Table 5 Calculation results for $CaMg_2N_2$ (experimental values from ref 11 are given in parentheses): Values of the trigonal cell parameters, atomic fractional coordinates, major interatomic distances and calculated band gap

Cell parameters SG $P\bar{3}m1$ (VASP results)/Å	Atomic fractional coordinates (VASP results)	Interatomic distances (VASP results)/Å	Expected band gap/eV	Calculated band gap/eV
a = 3.5497 (3.5405)	Ca 0 0 0.5	Ca–N 2.613 × 6 (2.595 × 6)	>3.1 (colorless)	2.05 (WIEN97)
c = 6.1029 (6.0908)	Mg 1/3 2/3 0.8584	Mg–N 2.126 × 3 (2.129 × 3), 2.2949 × 1 (2.296 × 1)		2.27 (VASP)
	N 1/3 2/3 0.2345	Ca···Mg 2.997 (2.999)		
		Ca···Ca 3.549		
		Mg···Mg 2.681 (2.659)		

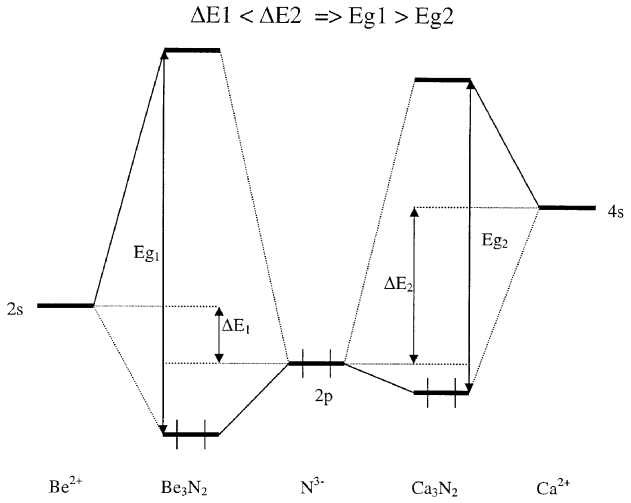

Fig. 8 Simple orbital scheme, taking into account the strong covalent interaction which exists between M^{2+} and N^{3-} and which is responsible for the difference between the Be_3N_2 and Ca_3N_2 band gaps (Eg).

$CaMg_2N_2$ in which Mg is tetracoordinated, is not that much larger than that of α-Mg_3N_2.

Finally, it should be pointed out that these computed results are consistent with the available experimental data reported in Table 4. Band gaps obtained from diffuse reflectance experiments are available in the case of M = Mg and Ca. For Mg_3N_2, Fang *et al.* measured an energy gap of about 2.8 eV.[5] On the other hand, we have experimentally determined the optical gap of Ca_3N_2 (1.9 eV). Although no experimental data is available for α-Be_3N_2 and $CaMg_2N_2$, their white color indicates a band gap larger than 3.1 eV. If one takes into account that DFT always underestimates the size of the gaps,[19] the variations of the experimental and calculated band gaps are fully consistent, at least at a semi-quantitative level.

References

1 M. Jansen, E. Guenther and H. P. Letschert, *Ger. Pat.*, 199 07 618.9, 1999.
2 M. Jansen, H. P. Letschert and D. Speer, *Eur. Pat.*, 592876, 1993.
3 K. Nassau, *Color for Art, Science and Technology, Azimuth 1*, Elsevier Science B.V., Amsterdam, 1998.
4 Ma. Guadalupe Moreno Armanta, A. Reyes-Serrato and M. Avalos Borja, *Phys. Rev. B*, 2000, **62**, 4890.
5 C. M. Fang, R. A. de Groot, R. J. Bruls, H. T. Hintzen and G. de With, *J. Phys.: Condens. Matter*, 1999, **11**, 1.
6 D. H. Gregory, *Coord. Chem. Rev.*, 2001, **215**, 301.
7 M. von Stackelberg and R. Paulus, *Z. Phys. Chem., Abt. B*, 1933, **22**, 305.
8 A. V. Antropoff and K. H. Krüger, *Z. Phys. Chem., Abt. A*, 1933, **167**, 49.
9 A. Guntz and F. Benoit, *Ann. Chim. (Paris)*, 1923, **20**, 5.
10 J. Gaudé and J. Lang, *C. R. Seances Acad. Sci., Ser. C*, 1972, **274**, 521.
11 V. Schultz-Coulon and W. Schnick, *Z. Naturforsch., B*, 1995, **50**, 619.
12 D. E. Partin, D. J. Williams and M. O'Keeffe, *J. Solid State Chem.*, 1997, **132**, 56.
13 A. M. Heyns, L. C. Prinsloo, K.-J. Range and M. Stassen, *J. Solid State Chem.*, 1998, **137**, 33.
14 G. Kresse and J. Furthmuller, *Phys. Rev. B*, 1996, **54**, 11169.
15 J. P. Perdew, J. A. Chevary, S. H. Vosko, K. A. Jackson, M. R. Pederson, D. J. Singh and C. Hollais, *Phys. Rev. B*, 1992, **46**, 6671.
16 P. Blaha, K. Schwartz and J. Luitz, *WIEN97, A Full Potential Linearised Plane Waves Package for Calculating Crystal Properties*, Karlheinz Schwartz Techn. Universität Wien, Austria, 1999 (ISBN 3-9501031-0-4).
17 J. P. Perdew, K. Burke and M. Ernzerhof, *Phys. Rev. Lett.*, 1996, **77**, 7865.
18 R. O. Jones and O. Gunnarsson, *Rev. Mod. Phys.*, 1989, **61**, 689.
19 E. Orhan, J.-Y. Saillard and R. Marchand, unpublished results.